

Particle Trajectory Tracing in the Geomagnetic Field

Ming-Huey A. Huang, Shih-Chang Lee, Ping Yeh, Zhongliang Ren, and Yao-Li Chuang

Institute of Physics, Academia Sinica, Taipei, Taiwan 115, R.O.C.

(Received October 29, 2000)

The particles detected in a near Earth orbit could be primary cosmic rays, trapped radiation, or albedo particles produced in the atmosphere. To understand the origin of these particles, we have developed a set of programs to trace charged particles in the geomagnetic field. The algorithm and the model of the geomagnetic field adopted are described in this article. The numerical errors are studied in two ways, as a function of either the tracing time or the gyration step size. An optimal step size of 0.04 rad is selected for further analyses. Using this program, we studied the data obtained by the Alpha Magnetic Spectrometer and were able to differentiate cosmic rays from atmospheric secondary particles.

PACS. 07.05.Tp – Computer modeling and simulation.

PACS. 94.30.Bg – Magnetic coordinate systems.

PACS. 94.30.Hn – Trapped particles.

I. Introduction

There are two known components of space radiation: primary cosmic rays and trapped radiation. The geomagnetic field provides a shield from bombardment by the low energy cosmic rays. Below the rigidity cutoff, the cosmic rays can not penetrate the geomagnetic field to reach the ground. The rigidity cutoff provides a separation of the primary cosmic rays and the trapped particles.

Particles above and below the rigidity cutoff had been observed since the 1950's. Many rocket and satellite experiments have explored the radiation belts thoroughly. The Van Allen radiation belts are known to be composed of particles trapped inside the geomagnetic field. The energy spectrum was measured up to 600 MeV, well below the rigidity cutoff near the equator. The motions of the trapped charged particles are well studied in space physics [1].

The Alpha Magnetic Spectrometer (AMS) is a space borne particle detector designed to detect antimatter, dark matter, and cosmic rays [2]. In June 1998, the AMS had a test flight on board the space shuttle Discovery. During 10 days of flight, AMS triggered and recorded some 10^8 events. Besides the primary cosmic rays, a second spectrum below the geomagnetic rigidity cutoff was clearly seen [3, 4]. The energy of this second spectrum reaches the order of GeV, close to the rigidity cutoff and much higher than the previous measured energy spectrum in the radiation belts.

Anti-protons and positrons can be generated inside the atmosphere and rebound to space, becoming so called “*albedo particles*”. It is important to distinguish these albedo particles from the primary cosmic rays. AMS can determine the particle trajectory with high precision, therefore

it is possible to trace the trajectory of a detected particle backward in time in the geomagnetic field to find its origin.

To understand the origin of the particles detected by AMS and the effect of the rigidity cutoff, we have developed a set of programs to trace the trajectory of charged particles in the geomagnetic field. The geomagnetic field models and the coordinate system are described in section II. In section III, the algorithm and the main features of the tracing programs are discussed. Using this programs, particles near and below cutoff detected by AMS are traced and their origins are discussed in section IV.

II. Models of the geomagnetic field

The geomagnetic field consists of two parts, the main field produced by the internal magnetic moments of the Earth and the external field driven by the solar wind plasma. In this study, we focus on the particle trajectory in a time scale of less than a few minutes. The time scale of the secular variation, the lunar variation, and the diurnal variation are much longer, so that the internal field can be regarded as a static field. Although the external field produces anisotropic distribution in the day and the night sides of magnetosphere and have effects at altitudes larger than 7 times of the mean Earth radius, $R_E = 6371.2$ km, the flight path of AMS covers the L-shell [1] only up to $L=6.4$, i.e. the highest altitude of magnetic field line is $6.4 R_E$. For space experiments on the low orbits such as AMS on space shuttle or space station, the main field alone is sufficient for studying the behavior of particles below cutoff. In this study, only the main field is used in the modeling of the geomagnetic field.

II-1. Main geomagnetic field

Because the main field is static, it can be modeled by a polynomial of spherical harmonics,

$$V = a \sum_{n=0}^{\infty} \frac{a_n}{r^{n+1}} \sum_{m=0}^{\infty} P_n^m(\cos \mu) (g_n^m \cos m\tilde{A} + h_n^m \sin m\tilde{A}) \quad (2.1)$$

and the magnetic field $\mathbf{B} = -\nabla V$. The International Geophysics Union publishes the fitted coefficients, g_n^m and h_n^m , to the 10th degree. This model is called the International/Definitive Geomagnetic Reference Field (IGRF/DGRF) [5]. Similar sets of coefficients, DoDWMM, are produced jointly by the British Geological Survey (BGS) and the U.S. Geological Survey, and fit the data to the 12-th degree [6]. For AMS, we use the 1995 data sets and extrapolate to June 7, 1998, the median date of AMS shuttle flight.

As shown in Figure 1, the difference between the DoD-WMM95 model and the IGRF95 model, is less than ≈ 300 nT or 0.6%. Since this is of the same order as the diurnal variation, it can be safely neglected. We use the DoD-WMM95 model in this work.

II-2. Magnetic coordinate

In a realistic geomagnetic field model, the spatial coordinates are expressed with Corrected GeoMagnetic coordinate (CGM). The CGM coordinate is defined by the following procedures. Starting from a desired location, follow the realistic field line to the dipole equator, then return to the same altitude along the dipole field line. The dipole coordinate of the final position is the CGM coordinate of the starting point [7].

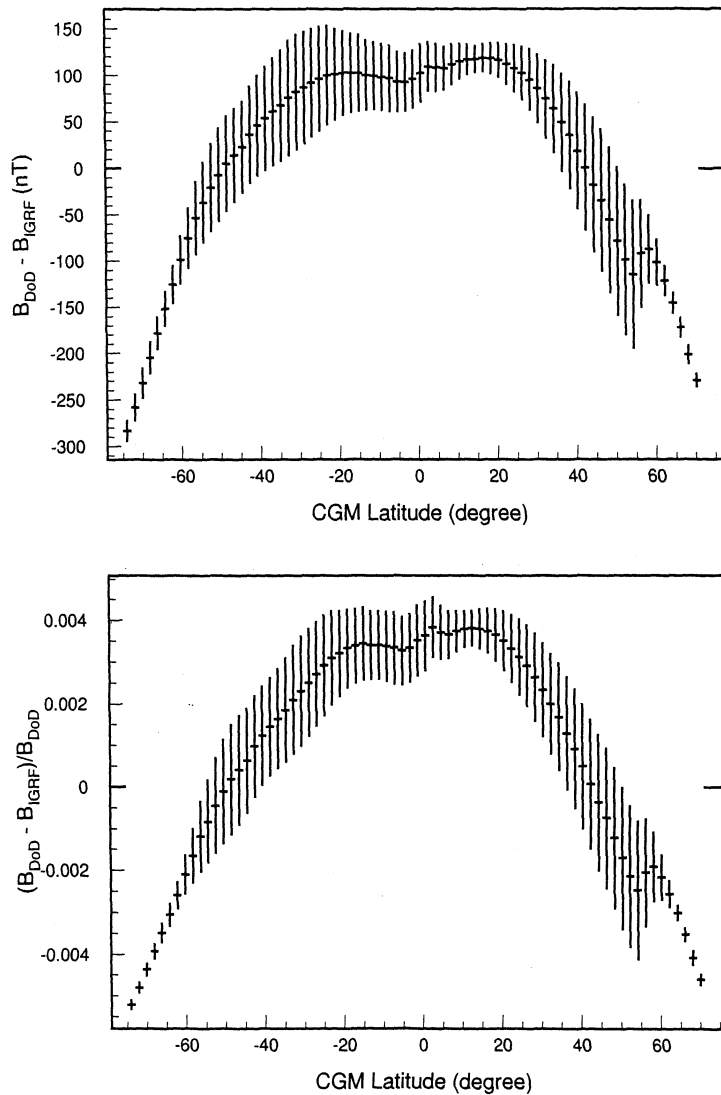


FIG. 1. The geomagnetic field strength are calculated by IGRF95 and DoDWMM95 in a $1^\circ \times 1^\circ$ grid at altitude 370 km above the mean sea level. The mean value and RMS width of the difference between two models over all longitude are plotted as a function of latitude in top figure. The bottom figure show the mean value and RMS width of relative difference.

In some areas, (the forbidden zone), the field lines do not cross the dipole equator, therefore the CGM algorithm can not be applied to calculate the magnetic coordinate. Instead, a Constant B-Minimum (CBM) coordinate developed by N. Papitashvili and V. Papitashvili [8] is used in these areas. However, in some areas the magnetic field line are distorted by Earth crust and mantle and have difficulty to find the B-minimum. A linear interpolation of CBM coordinates of adjacent points along the same longitude is used. This approach may map different geographic coordinates

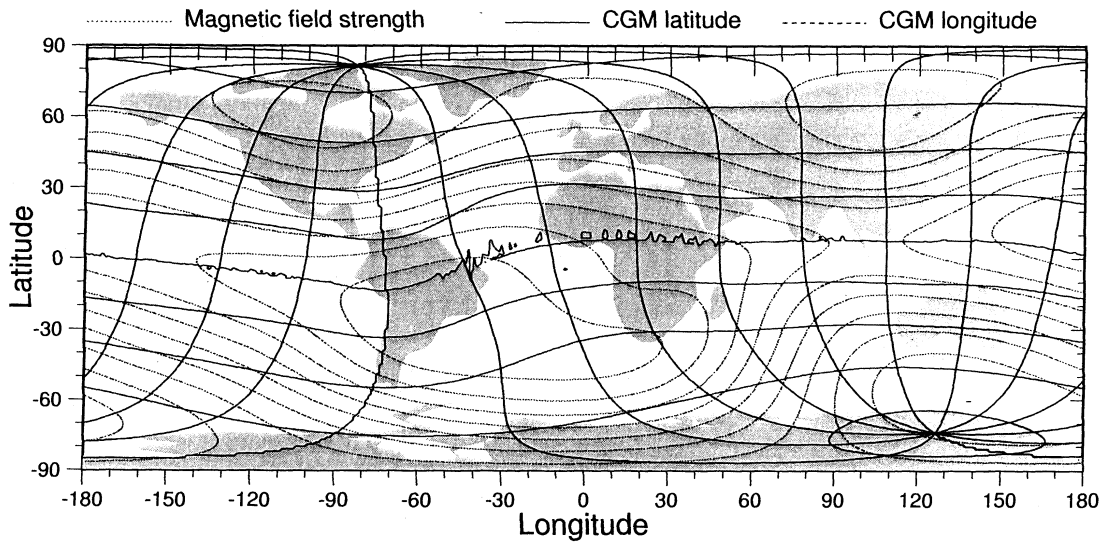


FIG. 2. Contour of geomagnetic field strength and contour of magnetic latitude and longitude at 40km above sea level.

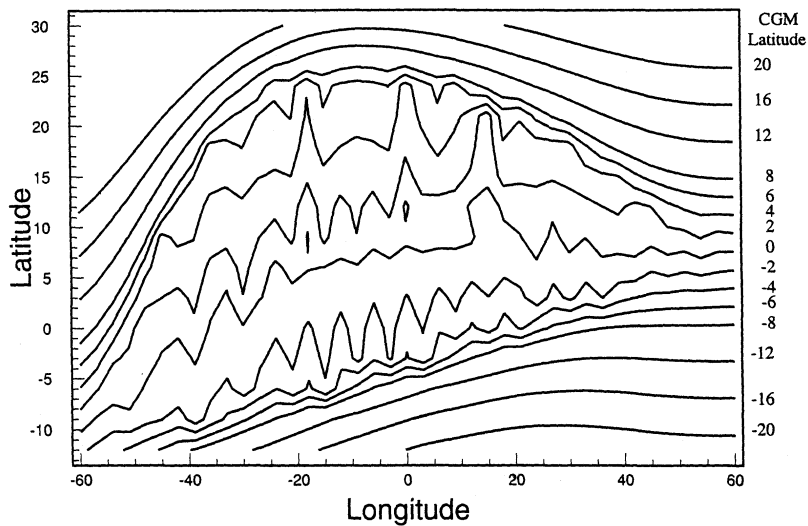


FIG. 3. The area where CGM latitude are ill-defined. In the program GEOPACK96, these region can be identify by a return variable PMI=999.

into one single CGM coordinate. That is, the mapping is irreversible. The source codes, GEOPACK-96, which implement the above algorithms are available on the web [5, 9]. The magnetic coordinates are plotted in Figure 2.

The problem inside forbidden zone is most serious in the equator at the longitudes between

$\pm 60^\circ$, as shown in Figure 3. Apparently, the jitters shown in Figure 3 are unphysical results produced by the interpolation of the CBM approach. In the realistic case, the magnetic equator varies due to the diurnal variation of geomagnetic field. It is impossible to have a fix position of magnetic equator. The magnetic coordinate inside forbidden zone is a known question for geophysicist. Some alternative algorithms are also proposed, each have different advantages and disadvantages. The CGM+CBM coordinates provide coverage over larger space and reasonable value inside forbidden zone. However, limitation must be remembered. We use the CGM-latitude $j_{\text{CGM}} < 0.2$ rad to define the equatorial region.

III. Particle trajectory tracing

III-1. Algorithm of tracing

The equation of motion of a charged particle in a magnetic field can be written in the form of a first-order 6-dimensional ordinary differential equation in the phase space $(\mathbf{r}; \mathbf{p})$.

$$\frac{d\mathbf{r}}{dt} = \frac{\mathbf{p}}{m\gamma}$$

$$\frac{d\mathbf{p}}{dt} = \frac{q}{m\gamma} \mathbf{p} \times \mathbf{B}$$

where $\mathbf{r}; \mathbf{p}$ are vectors of the position and momentum of the particle, m is the rest mass, q is the charge, and γ is the relativistic gamma factor.

The solution are numerically integrated by the fourth order Runge-Kutta method. The step size in time, Δt , is calculated such that the particle would turn an angle of $\Delta\theta$, called the gyration step size, in the local \mathbf{B} field, that is,

$$|\mathbf{v}| \Delta t = \Delta\theta \frac{|\mathbf{p}|}{qB}$$

This has an advantage that the particle can “leap” to save computation time when it is in a region of weak \mathbf{B} fields, and it can make very small steps when \mathbf{B} field is strong where large steps results in large errors.

III-2. Error estimation

To study the numerical error induced by the tracing as a function of tracing time T , we trace particle forward in time for $T/2$ seconds, then trace backward for another $T/2$ seconds. If there is no accumulation error, the particle would return to its starting point. The numerical error is estimated with the shortest distance between the starting point and the returning path. Figure 4 shows the distribution of the accumulated error for 10 seconds of tracing for a random sample of particles. Figure 5 shows the relation of the mean error as a function of the tracing time. At gyration step size $\Delta\theta = 3$ mrad, it can be approximated by $\Delta x = 0.05 \Delta T^2$ km.

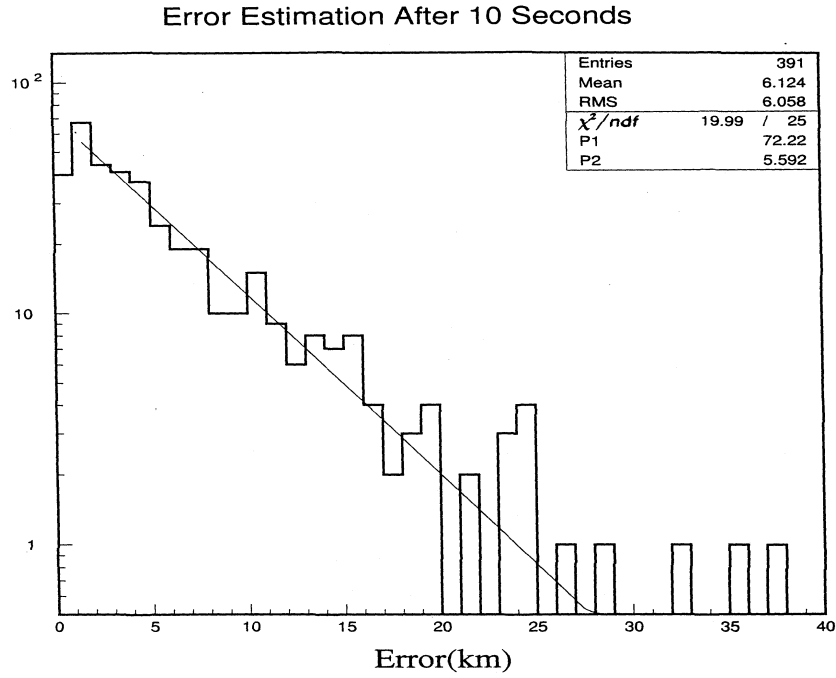


FIG. 4. The accumulated error of forward and backward tracing for 10 seconds

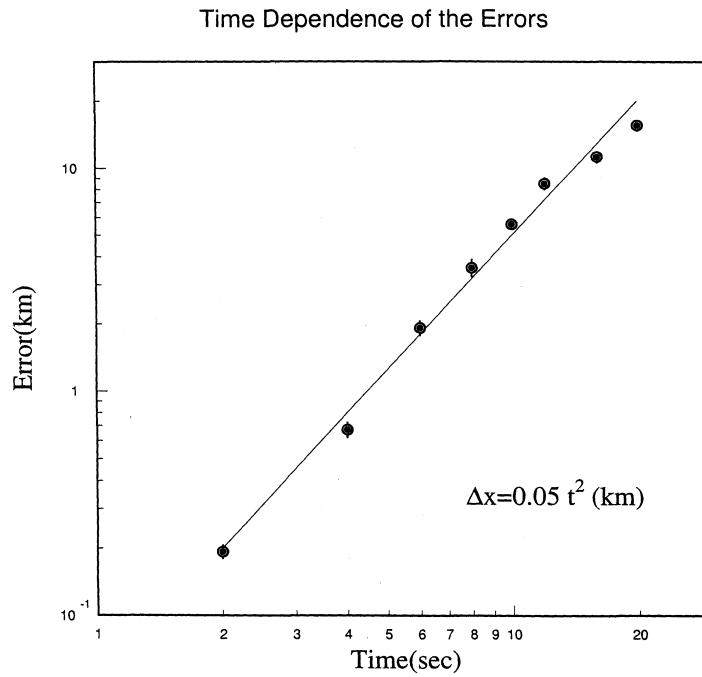


FIG. 5. The accumulated error of as function of tracing time using gyration step size 3 mrad.

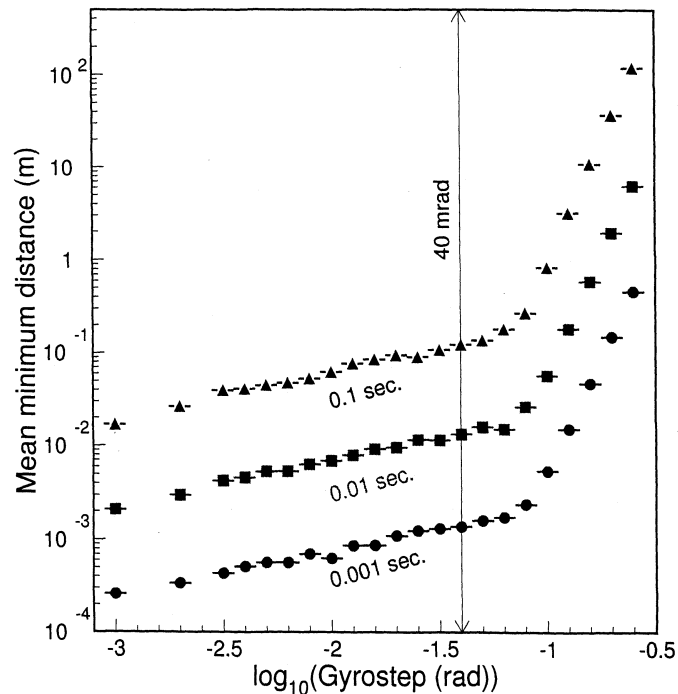


FIG. 6. The accumulated error of as function of gyration step size for several tracing time.

Figure 6 shows the relation of the mean error as a function of gyration step size. It can be seen that above a certain step size, the error increases sharply. The larger the step size, the shorter the computing time. The optimal choice of the step size depends on balancing the requirements of smaller error and shorter computing time. For our study, we chose $\phi = 40$ mrad. For this step size, the mean error can be approximated by $\pm x = 0.7 \ell T^2$.

IV. Atmospheric secondary particles

IV-1. General feature of trajectory tracing

The Earth's surface is assumed to be an ellipsoid of polar radius 6356.75 km and equatorial radius 6378.13 km. The boundary of the main geomagnetic field is assumed to be $10 R_E$, the approximate size of magnetopause in the Sun facing direction. In the current static geomagnetic field model, $10 R_E$ can be assumed to be the mean distance over different time of the day.

The energy loss of a particle due to collisions and ionization with air nuclei is ignored. The top of the atmosphere is assumed to be 40 km above the mean sea level. 40 km is about the floating altitude of most of the balloon experiments. The vertical depth of the residual atmosphere at the altitude 40 km is approximately 5 gm/cm^2 . When particles enter the top of the atmosphere, they penetrate to lower atmosphere and lose energy quickly.

The trajectory tracing can be done either backward or forward in time. Particles are classified as cosmic rays when they escape to an altitude greater than $10 R_E$ during backward tracing. To avoid large energy losses, the source position of a secondary particle is where the

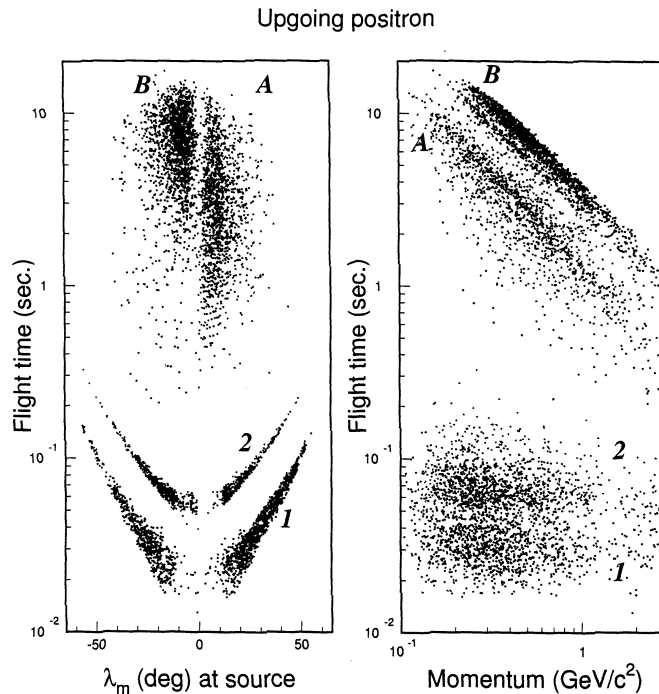


FIG. 7. The left figure shows total life time vs magnetic latitude at source of secondary positrons. The two horizontal arches are short flight time particles correspond to magnetic equator crossing once or twice. These are the short flight time particles. The upper part, flight time > 0.2 sec., are separated to (A) northern hemisphere and (B) southern hemisphere. The right figure show the flight time vs momentum of secondary positrons. Above 0.2 second, the long flight time particles have flight time approximately inverse proportional to kinetic energy.

particle hit the 40 km during backward tracing while the sink position is where the particle hit the 40 km during forward tracing. Cosmic rays are distinguished from secondary albedo particles by their source position. The albedo particles come from altitude below 40 km. The trapped particles are defined as particles survive in between above 40 km and below $10 R_E$ for more than one drift period [1].

IV-2. Secondary electrons and positrons detected by AMS

Using the trajectory tracing program that we developed, we studied the AMS data of protons with momentum less than 6 GeV/c and all the electrons and positrons. At high latitude, many of these particles are cosmic rays of origin. The rest are albedo particles, which hit both the 40 km altitude and the ground level when traced both forward and backward in time. No trapped particles are identified in the data collected by AMS. Many of those albedo particles are positrons, which are anti-particles and can only be produced by the high energy interaction of primary cosmic rays with atmospheric nuclei.

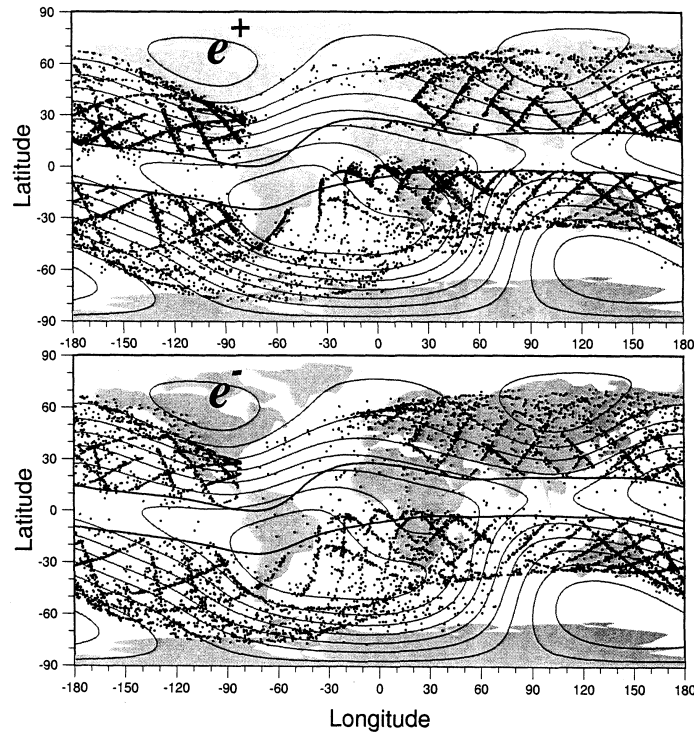


FIG. 8. The source of short flight time electrons and positrons. The contour lines are the magnetic field strength at the altitude 40 km above geoid. The data when AMS flight over South Atlantic anomaly are excluded because of large dead time. This is reflected by the void in the north Atlantic $80^\circ < \text{longitude} < 30^\circ$ in this figure. The equatorial gap can be approximate by magnetic latitude $\lambda_m = \pm 12^\circ$, shown by two solid line near equator.

$$\begin{aligned}
 & \text{H, He, ... + N}_2 ; \text{O}_2 ; \dots ; \text{!} \quad \text{H} = \frac{1}{4} \text{O}^{\text{S}} = \text{K}^{\text{O}^{\text{S}}} \dots + \dots \\
 & \frac{1}{4} \text{O}^{\text{S}} ; \text{K}^{\text{O}^{\text{S}}} ; \text{!} \quad \text{e}^+ ; \text{e}^- + \dots
 \end{aligned}$$

These albedo particles must be atmospheric secondary particles.

The total time from the source to the sink is defined as the flight time of the secondary particle. Figure 7 shows the flight time as a function of the magnetic latitude and momentum of the positron. Two distinct groups show up. One consists of short flight time particles ($T \ll 0.2\text{s}$ for e^{S} and $T \ll 0.3\text{s}$ for proton) with the flight time being nearly independent of momentum; the other consists of long flight time particles with the flight time being approximately inversely proportional to the momentum.

The short flight time particles bounce a couple of times between the north and the south magnetic hemispheres. Since these particles are created and absorbed by atmosphere in a very short time, their source and sink positions follow the magnetic field line of the guiding center to the ground. Therefore the distribution of sources and sinks have a pattern similar to the flight

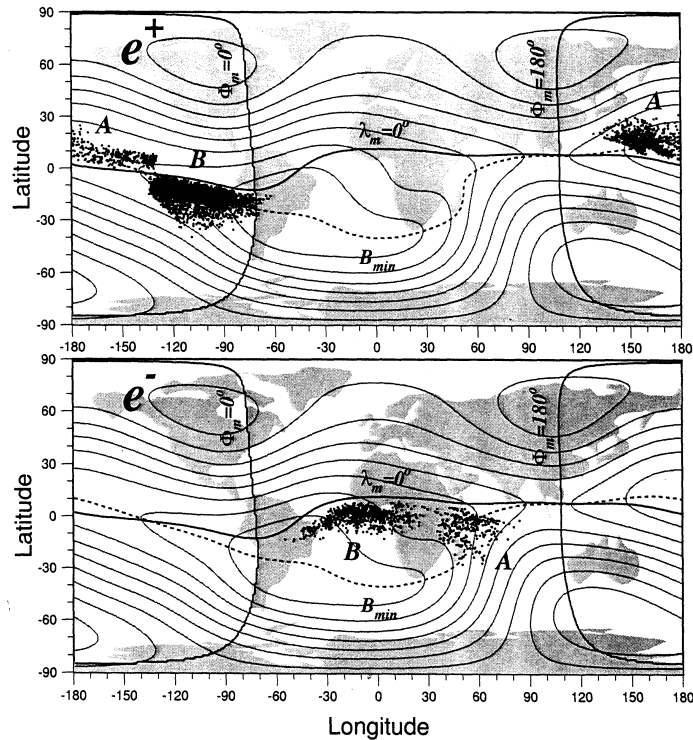


FIG. 9. The source of long flight time electrons and positrons. The contour lines are the magnetic field strength at the altitude 40km above geoid. The magnetic equator ($\lambda_m = 0^\pm$, defined by minimum of L-shell along a geographic meridian) and the position of minimum magnetic field strength (B_{min}) are also shown. Notice that the source are all in the same side of minimum magnetic field strength. λ_m is the CGM longitude. The source of long flight time positrons and electrons are separated in two side of $\lambda_m = 0^\pm$.

path of the detector. Figure 8 shows the source of the short flight time secondary electrons and positrons. There is an equatorial gap in between the CGM-latitude $\approx 12^\pm$. Inside the gap, the local magnetic field lines at top of atmosphere can not reach the AMS altitude. Outside the equatorial gap, the distribution of sources is approximately uniform.

The long flight time particles are produced near 0^\pm in CGM-longitude, λ_m where the magnetic field strength is the weakest along magnetic equator. These particles drift over $\lambda_m = 180^\pm$ where their altitude are highest and then descend when returning to $\lambda_m = 0^\pm$. This drift motion increases the flight time to the same order of drift period of the particle. The source and sink of these particles form two regions, east and west of $\lambda_m = 0^\pm$. This can be understood as the result of the offset of the center of geomagnetic dipole from the center of the Earth. Figure 9 shows the source and sink of the long flight time secondary electrons and positrons. Notice that the source of the electron (positrons) is identical to the sink of the positrons (electrons). Because electrons drift westward and positrons drift eastward, so that only electrons originate at the west of $\lambda_m = 0^\pm$ and the positrons originate at the east of $\lambda_m = 0^\pm$ survive and become long flight time particles.

V. Summary

A particle trajectory tracing program is developed. It can be used to distinguish the primary cosmic rays from the atmospheric albedo particles. We had made extensive studies on the accumulated error of this program. The optimal choice of gyration step size is selected as 40 mrad and the mean error $\pm X$ can be approximated by $\pm X = 0.7 \text{ E T}^2 \text{ km}$, where T is the tracing time.

Using this tracing program, we traced particles in the data taken by the Alpha Magnetic Spectrometer and found many interesting features from particles below rigidity cutoff. We discovered that within the acceptance of AMS detector and energy range (0.1 GeV to 200 GeV), there are no trapped particles. Instead of having trapped particles flying in the vicinity of the Earth, the secondary albedo particles are produced and absorbed by the atmosphere constantly to reach a steady flux.

These atmospheric secondary particles can be categorized in two groups, short and long flight time, by the total flight time outside atmosphere. The short flight time particles are related to the bounce motion and the long flight time particles are related to the drift motion [10]. The behavior of these below cutoff particles are similar to the trapped particles in the radiation belts. They also populate in the same region of radiation belts. However, the flight time are quite different and origin might be different too. Details of the study of the atmospheric secondary particles will be published later.

Acknowledgments

This work was supported in part by the National Science Council of the Republic Of China under the grants NSC-88-2112-M-001-034 and NSC-89-212-M-001-043. We thank Dr. Yeh, Huey-Ching for the discussions on the geomagnetic coordinates.

References

- [1] M. Walt, *Physics of geomagnetically trapped radiation*, (Cambridge University Press, Cambridge, 1994).
- [2] S. Ahlen *et al.*, Nucl. Inst. Meth **A419**, 295-299 (1994).
- [3] AMS collaboration, Alcaraz, J. *et al.*, Phys. Lett. **B472**, 215 (2000).
- [4] AMS collaboration, Alcaraz, J. *et al.*, Phys. Lett. **B484**, 10-22 (2000).
- [5] <http://nssdc.gsfc.nasa.gov/space/model/>
- [6] <http://www.ngdc.noaa.gov/seg/potfld/magmodel.shtml>.
- [7] Hultqvist, B. Arkiv. for Geofysik **3**, 53 & 63, (1958); Gustafsson, G. Arkiv. for Geofysik **5**, 595 (1970).
- [8] Gustafsson, G., N. E. Papitashvili, and V. O. Papitashvili, J. Atmos. Terr. Phys. **54**, 1609-1631 (1992)
- [9] <http://www-spf.gsfc.nasa.gov/Modeling/geopack.html>
- [10] M. A. Huang, Proc. of the 8th Asia Pacific Physic Conference, Taipei, Taiwan, Aug. 7-10, 2000, astro-ph/0009106.